processes

MDPI

Article

Influence of Organic Ligands on the Colloidal Stability and Removal of ZnO Nanoparticles from Synthetic Waters by Coagulation

Rizwan Khan [1], Muhammad Ali Inam [1], Du Ri Park [1], Saba Zam Zam [1], Sookyo Shin [1], Sarfaraz Khan [2], Muhammad Akram [3] and Ick Tae Yeom [1,*]

1 Graduate School of Water Resources, Sungkyunkwan University (SKKU) 2066, Suwon 16419, Korea; rizwankhan@skku.edu (R.K.); aliinam@skku.edu (M.A.I.); enfl8709@skku.edu (D.R.P.); sabazamzam@skku.edu (S.Z.Z.); tkssk08@gmail.com (S.S.)

2 Key Laboratory of the Three Gorges Reservoir Region Eco-Environment, State Ministry of Education, Chongqing University, Chongqing 400045, China; Sfk.jadoon@yahoo.com

3 Shandong Key Laboratory of Water Pollution Control and Resource Reuse, School of Environmental Science and Engineering, Shandong University, Qingdao 266200, China; m.akramsathio@mail.sdu.edu.cn

* Correspondence: yeom@skku.edu; Tel.: +82-31-299-6699

Received: 1 September 2018; Accepted: 15 September 2018; Published: 17 September 2018

Abstract: The large-scale production and usage of zinc oxide nanoparticles (ZnO NPs) may lead to their post-release into the aquatic environment. In this study, the effect of hydrophobic/hydrophilic organic ligands on sorption and sedimentation of ZnO NPs has been systematically investigated. In addition, the coagulation efficiency of ZnO NPs, Zn^{2+}, dissolved organic carbon (DOC), and UV_{254} with varying ferric chloride (FC) dosages in synthetic waters were also evaluated. The results showed that the higher concentration of organic ligands, i.e., humic acid (HA), salicylic acid (SA), and L-cysteine (L-cys) reduced the ζ-potential and hydrodynamic diameter (HDD) of particles, which enhanced the NPs stability. The adsorption of organic ligands onto ZnO NPs was fitted with the Langmuir model, with maximum adsorption capacities of 143, 40.47, and 66.05 mg/g for HA, SA and L-cys respectively. Removal of up to 95% of ZnO NPs and Zn^{2+} was achieved in studied waters at the effective coagulation zone (ECR), above which excess charge induced by coagulant restabilized the NPs in suspension. Moreover, the removal rate of DOC and UV_{254} were found to be higher in hydrophobic waters than hydrophilic waters. The width of ECR strongly depends on the characteristics of source water. The waters with hydrophobic ligand and higher UV_{254} values require more coagulant than hydrophilic waters to achieve the similar ZnO NPs and Zn^{2+} removal. The results of Fourier transform infrared (FT-IR) analysis of ZnO NPs composite contaminant flocs indicated that the combined effect of enmeshment and charge neutralization might be a possible removal mechanism. These findings may facilitate the prediction of fate, transport, and removal of ZnO NPs in the natural waters, and might contribute to risk assessment, as well as decision making about engineered nanoparticles (ENPs) in aquatic systems.

Keywords: adsorption; coagulation; organic ligands; stability; water treatment; ZnO NPs

1. Introduction

The engineered nanoparticles (ENPs) are extensively used in commercial products, with applications in industrial processes, electronics, agricultural and environmental sciences, mainly because of their unique structural properties compared to conventional bulk materials [1,2]. It is estimated that about 35% of the globally-produced ENPs are released into the aquatic system, which leads to the high possibility of their co-presence in natural water sources [3]. Amongst several inorganic ENPs, zinc oxide nanoparticles

(ZnO NPs) have been a widely used nanomaterial (NM) in the field of nanotechnology such as cosmetics, sunscreens, paints, pigments, foods, and medicines [4]. A recent study suggested that around 8–20% of the annual production of ZnO NPs (31,500–34,000 t/y) may inevitably enter into the water environment [5]. Moreover, few researchers have reported that the concentration of NPs in surface water in the U.S could be up to 50–10,000 ng/L, which is anticipated to increase over time with higher use and disposal of the NP-containing products [1,6]. Therefore, there is growing concern regarding the likelihood of the occurrence of these NPs in drinking water sources, and the potential increased risk of exposure to humans as well as the aquatic environment.

In the aquatic system, aggregation and dissolution of NPs are the critical factors in evaluating their hazards and associated toxicity exposure risk. The toxic effects of ZnO NPs on various aquatic biota, including daphnia, sea urchin, algae, plants, and mammalians, were reported in the literature [7,8]. Additionally, the adverse effects of these NPs were also reported on humans, including damage to DNA and cell membranes [9]. The ability of these NPs to penetrate via ingestion into the body and cell (via fluid-phase endocytosis and caveolae) may provide an accessible site to these toxic NPs as well as Zn^{2+} pollutants [10]. The toxicity and bioavailability of NPs also depend upon their physiochemical properties, including size, surface charge, and other components of waters, i.e., pH, organic ligands and inorganic ions. Small NPs have higher mobility due to the effect of hydrodynamic forces, and more active reaction sites increase the risk to organisms as compared to larger NPs that are aggregated [11]. Likewise, the metal cations enhance aggregation by neutralizing charges, subsequently adsorbing onto the NPs surface [12]. In contrast, naturally ubiquitous organic ligands like humic acid (HA), salicylic acid (SA) and L-cysteine (L-cys) can adsorb onto the surface of NPs unselectively via ligand exchange, hydrophobic/hydrophilic interaction, and H-bonding, which promotes the stability of NP suspension and bioaccumulation [13,14]. Some recent studies have focused on the effect of physicochemical properties of organic ligands, i.e., molecular weight (MW) distribution and hydrophobic/hydrophilic characteristics on NPs dissolution and aggregation [15,16]. The elevated concentration of hydrophobic, high molecular weight (HMW) ligands like HA consists of abundant hydroxyl, carboxyl, and phenolic groups, which enhance the dissolution of NPs [15]. Our previous study [17] has shown the high aggregation kinetics of ZnO NP suspensions in the presence of a hydrophilic, low molecular weight (LMW) ligand such as SA containing carbohydrates, and other active groups. Similarly, the adverse effects of hydrophilic, LMW ligands, like L-cys containing thiol groups, on NPs aggregation has also been reported [18]. In contrast, some researchers have shown that in a complex system, the L-cys produces a reactive insoluble thiol complex which strongly binds to metal ions, thus alleviating the aggregation and reducing the toxicity of NPs to a certain extent [13]. It has also been found that the lysine consisting of cysteine modified the surface of NPs, and further improved the stability of silver (Ag) NPs [14]. Therefore, the stability and aggregation behavior of NPs depends upon their specific interactions with several components present in natural waters.

The presence of NPs in the aquatic system may provide a potential route for human exposure, primarily if the source is used as potable water. The conventional water treatment coagulation/flocculation/sedimentation is an efficient and economical process to remove the colloidal particles, organic matters, inorganic compounds, and heavy metal ions from water. Previous studies [19–22] demonstrated that NPs such as CdTe, C_{60}, Ag, and titanium dioxide (TiO_2) could be removed from water by polyaluminum chloride (PACl) and alum coagulation. Moreover, variable coagulation efficiencies of metal oxide NPs, including ZnO (48–99%), Ag (2–20%) and TiO_2 (3–8%) have been studied [23]. Recently a group of researchers has demonstrated the efficient removal of ZnO and CuO NPs through a combination of a high dosage of PACl and a coagulant aid [24,25]. The removal of heavy metal ions Zn, Cu, and cadmium (Cd) from the single as well as binary aqueous systems through batch adsorption experiments have also been reported [26,27]. The results of analytical models and experimental data suggested that the adsorption capacity of Zn is not influenced by the presence of other interfering ions in a heterogeneous system. Some previous studies showed that the presence of complex aqueous ligands might reduce the adsorption capacity of Fe-oxide-coated quartz sand by changing the solid-to-solution ratio (SSR) in the aquifer [28].

Moreover, organic ligands have been proved to hinder aggregation and effect the removal performance of NPs during coagulation [20,22]. For instance, metal oxides coated with organic ligands such as HA and SA exhibited significant sorption abilities with enhancing stability, thus decreasing the NPs removal rate due to electrostatic/steric hindrance effect of adsorbed organic contaminants [29]. Conversely, enhanced NP precipitation was observed in the presence of thiolate functional groups caused by steric effects and a change in reaction rate [18]. However, studies reported in the literature are limited to NP removal in the presence of single organic ligands. Previous literature also seems insufficient regarding the specific interaction of the hydrophobic/hydrophilic organic ligand on the colloidal stability and behavior of ZnO NPs composite contaminant during coagulation.

The aim of this study is, therefore, to explore the effect of HA, SA, and L-cys on sorption ability and colloidal stability of ZnO NPs in various aqueous matrices. This work also hopes to evaluate the removal of ZnO NPs and Zn^{2+} by coagulation using ferric chloride (FC) from eight synthetic waters under laboratory condition. The yielded data was further used to predict the fate, mobility, and possible removal mechanism of ZnO NPs in natural waters.

2. Materials and Methods

2.1. Chemicals

The ZnO NP powder (mean particle diameter <50 nm), model organic ligands (humic acid, salicylic acid, and L-cysteine) was procured from the Sigma-Aldrich (St. Louis, MO, USA). The hydrochloric acid (HCl), sodium hydroxide (NaOH), nitric acid (HNO_3), sodium chloride (NaCl), magnesium chloride ($MgCl_2$) and iron (III) chloride hexahydrate ($FeCl_3 \cdot 6H_2O$) were purchased from Samchun (Samchun pure Chemicals Co., Ltd., Pyeongteak-si, Korea). Nanopure water (18.2 MΩ) was produced with Synergy ultrapure water system (Milli-Q, Millipore Co., Bedford, MA, USA), and used to prepare the stock as well as synthetic water solutions. All chemicals in this study were of reagent grade, and were used as received without any purification.

2.2. Experimental Procedure

2.2.1. Preparation of Stock Solutions

The ZnO NP suspension was prepared by adding 3 mg ZnO NPs powder in 100 mL nanopure water. The effect of ultrasonication time on the solution turbidity and particle size distribution were determined by turbidity measurements (Hach Benchtop 2100N, Loveland, CO, USA) after several optimization experiments. Before the experiment, all samples were subjected to probe sonication to disperse large NPs agglomerates using ultrasonic cell crusher (Bio-safer 1200-90, Â 12 mm, Nanjing, China). Humic acid (HA), salicylic acid (SA), and L-cysteine (L-cys) were used in this research to represent the hydrophobic, HMW, and hydrophilic, LMW organic ligands surrogate respectively. These model organic substances have widely been used to provide consistent experimental conditions [30]. The HA powder (1 g) was dissolved in 1 L of nanopure water, and the pH was adjusted to 10 using 0.1 M NaOH. The solution was stirred at 600 rpm for 24 h to ensure complete dissolution; then, the suspension was filtered by 0.45 µm glass fiber filter to remove insoluble particles. The 1 g/L stock solutions of SA and L-cys were prepared by dissolving the powder into 1 L of nanopure water. All stock solutions were stored in the dark at 4 °C in a refrigerator before being diluted to the desired experimental conditions.

2.2.2. Batch Sorption Experiments

The effect of organic ligand type and concentration (1–100 mg/L) on the ζ-potential and hydrodynamic diameter (HDD) of particles were evaluated. The adsorption kinetics of HA, SA, and L-cys (10 mg/L) on ZnO NPs (30 mg/L) were determined through a batch-equilibrium technique at 25 ± 1 °C. The suspensions were orbitally shaken at 100 rpm (Shaker, SK-300, Lab, Companion,

Kimpo, Korea) to simulate circulation conditions within natural surface waters, and sampled at intervals from 0.5 to 72 h. The supernatant of each mixture was filtered through a 0.2 μm glass fiber filter to measure the total organic carbon (TOC) content. Moreover, the adsorption kinetics of each organic ligand onto the ZnO NP surface were fitted with two commonly used Lagergren pseudo-first order (PFO) and Ho pseudo-second order (PSO) models using Equations (1) and (2) respectively.

$$\log(q_e - q_t) = \log q_e - \frac{k_1 t}{2.303} \quad (1)$$

$$\frac{t}{q_t} = \frac{1}{k_2 q_e^2} + \frac{t}{q_e} \quad (2)$$

where: q_e and q_t are the amounts of ligands adsorbed (mg/g) at equilibrium and at time t (h), respectively. k_1 and k_2 are rate constants adsorption (h^{-1}) of PFO and PSO models, respectively.

In addition, the stock solutions of each organic ligands were diluted in 100 mL vials to form a 50 mL experimental solution, where the dissolved organic carbon (DOC) concentration was maintained between 0 to 50 mg C/L. The pH of all experimental mixtures was adjusted to 7.0 with 0.1 M NaOH or 0.1 M HCl. The ZnO NPs-ligand suspensions were shaken at 100 rpm for 24 h, (based on the time study) to allow the suspension to equilibrate, and were then centrifuged at 10,000 rpm for 30 min. The supernatant was filtered, and the aliquot was collected for TOC analysis. Adsorption data were calculated assuming that the removal of the organic substances from suspension was due to the adsorption onto the NPs surface. Two of the most commonly-used isotherm (Langmuir/Freundlich) models were applied to fit the experimental data using non-linear Equations (3) and (4):

$$q_e = \frac{q_m K_L C_e}{1 + K_L C_e} \quad (3)$$

$$q_e = K_F C_e^{\frac{1}{n}} \quad (4)$$

where: q_e (mg/g) is the adsorbed amount of organic ligand on ZnO NPs at equilibrium; q_m (mg/g) and C_e (mg/L) is the maximum adsorption and equilibrium concentration of organic ligands. The K_L (L/mg) and K_F (L/mg) are the adsorption equilibrium constants of Langmuir for binding energy and Freundlich for adsorption capacity models respectively; n is heterogeneity factor for the Freundlich model, and shows the intensity of adsorption.

2.2.3. Preparation of Synthetic Waters

To investigate the effect of organic ligands on colloidal stability and the coagulation efficiency of ZnO NPs and Zn^{2+}, eight synthetic waters (S1–S8) with different DOC types and concentrations were synthetically prepared in the lab. The chemical characteristic of the raw water, i.e., specific ultraviolet absorbance (SUVA), is a significant indicator for defining the hydrophobicity/hydrophilicity and aromatic content of organic matter. Moreover, it also reflects a better reactivity of organic compounds present in waters towards removal by coagulation. It can be defined as the UV absorbance at 254 nm measured in (1/cm) divided by the DOC concentration measured in (mg/L). Therefore, the characteristics of hydrophobic and hydrophilic DOC were based on SUVA > 4 L/(mmgC) and < 3 L/(mmgC), respectively. In addition, the range of DOC concentration varied based on literature from low (1–2 mg C/L), moderate (2–3 mg C/L), and moderate-high (6 mg C/L) [31,32]. Based on the DOC values, two hydrophobic and six hydrophilic waters were prepared. The background ionic strength (IS) was controlled at 4.0 mM (1 mM IS NaCl, and 3 mM IS $MgCl_2$) to simulate moderately-hard water. The synthetic waters detail composition is presented in Table 1.

Table 1. The composition of the synthetically prepared waters.

DOC		Various Parameters of Synthetic Waters						
Type	**Concentration**	**Ligand Type & Water Code**		**DOC (mg C/L)**	**UV_{254nm} (1/cm)**	**SUVA (L/(mmg))**	**Turbidity (NTU)**	**EC (μS/cm)**
Hydrophilic SUVA < 3	Low-Moderate (ca. < 2 mg C/L)	SA	S1	1.62	0.017	1.04	1.05	158
		L-cys	S2	1.60	0.015	0.93	1.12	161
Hydrophilic SUVA < 3	Moderate (ca. 2–3 mg C/L)	SA	S3	2.69	0.035	1.30	1.21	375
		L-cys	S4	2.65	0.031	1.17	1.17	371
Hydrophobic SUVA > 4		HA	S5	2.58	0.195	7.55	5.06	378
Hydrophilic SUVA < 3	Moderate-high (ca. 6 mg C/L)	SA	S6	6.31	0.045	0.71	1.16	383
		L-cys	S7	6.18	0.037	0.60	1.20	382
Hydrophobic SUVA > 4		HA	S8	5.92	0.510	8.61	9.80	388

2.2.4. Dissolution and Sedimentation Measurements

The dissolution experiments of ZnO NPs (30 mg/L) spiked in pure and synthetic waters (S1–S8) were performed in a glass reactor for 24 h at 25 ± 1 °C. The buffer was not added to the ZnO NPs suspension to eliminate the potential effect of IS in this experiment. After 24 h, the solution of ZnO NPs and Zn^{2+} ions were separated by centrifugation at 10,000 rpm for 30 min, and the Zn^{2+} concentration in the supernatant was measured. To better understand the sedimentation behavior in natural waters, the aggregation kinetics of ZnO NPs in the synthetic waters were quantitatively determined by UV-Vis spectrophotometer. All spectra were collected using a 100 mm optical path length cuvette, which allows analysis of NPs at a relatively low concentration (2720.25 μg/L) [20]. The UV-Vis spectrum of ZnO NPs suspension (30 mg/L) over wavelength (200–800 nm) shows characteristic surface plasmon resonance band with a maximum located wavelength of 370 nm (see Supplementary Material Section S3.1 and Figure S1). The concentration of individual NPs was monitored through UV-Vis absorbance at 370 nm as a function of time for 24 h at different time intervals. In order to co-relate the NPs sedimentation process to the aggregation kinetics of ZnO NPs, the sedimentation theory by Stokes law was applied to estimate the settling rates of NPs in synthetic waters. According to Stokes' law, the settling velocity of spherical particles or floccules under gravitational forces is directly proportional to the square of the particle diameter [33]. The first-order kinetics model Equation (5) was obtained by fitting the NPs settling curve; Figure S4 shows that the first-order model fits the data well (R^2 = 0.9913). It is worthwhile to note the initial rapid decrease in normalized absorbance during fast settling which occurs within first 2 h followed by a slow aggregation within 24 h [34]. The effect of different ZnO NP concentrations (10, and 50 mg/L) on aggregation was also investigated for selected synthetic waters to determine the role of NPs concentration on aggregation.

$$\frac{dC}{dt} = -kC \rightarrow lnC_t = lnC_0 - kt \quad (5)$$

where C_t and C_0 is the absorbance at time t and 0; and k shows the sedimentation rate of NPs in the water phase. The graph of ZnO NPs aggregation was plotted as C_t/C_0 as coordinate and time (t) as abscissa.

2.2.5. Laboratory Jar Test Experiments with Synthetic Waters

The coagulation experiments were undertaken in 250 mL plexiglass beakers using jar tester (Model: SJ-10, Young Hana Tech Co., Ltd. Gyeongsangbuk-Do, Korea) with six paddles at 25 ± 1 °C. Before the coagulation process, the ZnO NP suspension prepared 1 mM $NaHCO_3$ solution was sonicated, as described in Section 2.2.1, and placed into the jars. Subsequently, samples were taken from each beaker for DOC, UV_{254}, ζ-potential, and turbidity analysis. The ferric chloride (FC) coagulant was dosed (0 to 0.50 mM), and pH was adjusted to a predetermined level. The coagulation was carried out in three sequential steps: initialization of coagulation by rapid mix at 200 rpm for 2 min; then, slow mix at 40 rpm for 20 min to enhance flocculation; and sedimentation for 30 min. After settling, an aliquot of 100 mL of the supernatant was sampled to analyze various solution parameters. The influence of the coagulant dose was investigated for all the studied waters at FC doses between 0 and 0.50 mM,

where 0 represents the control trial for each water. The average and relative standard deviation (RSD) were reported for triplicate analysis.

2.3. Other Analytical Methods

An aliquot of 30 mL was collected and centrifuged (Hettich Centrifuger Universal 320R, Tuttlingen, Germany) at 10,000 rpm for 30 min to separate the ZnO NPs and Zn^{2+} from suspension. The residual concentration of Zn^{2+} was analyzed by Inductively Coupled Plasma Optical Emission Spectroscopy (ICP-OES: Model Varian, Agilent Technologies, Santa Clara, CA, USA). The pH and conductivity of solutions were measured with (HACH: HQ40d Portable pH, Conductivity, Oxidation-Reduction potential (ORP) and Ion-Selective Electrode (ISE) Multi-Parameter Meter, Thermo Fisher Scientific, Waltham, MA, USA). The supernatant turbidity was measured to describe the physicochemical properties of studied waters. The concentration of organic matter was determined from UV_{254nm} (UV absorbance at 254 nm wavelength) using UV-Vis spectrophotometer (Optizen 2120 UV, Mecasys, Daejeon, Korea). The inorganic elemental analysis and TOC content were measured with a TOC analyzer with an ASI-L liquid autosampler (TOC-5000A, Shimadzu Corp, Kyoto, Japan). The electrophoretic mobility (EPM) and HDD of ZnO NPs were measured by laser Doppler electrophoresis and DLS using a Malvern Zetasizer (NanoZS, Worcestershire, UK). The Brunauer Emmett Teller (BET) surface area and pore size were determined through N_2 adsorption isotherms at −196 °C using a gas adsorption device (ASAP 2020, micromeritics, Norcross, GA, USA). The crystallinity of the ZnO NPs powder was studied using Rigaku D-max C III, X-ray diffractometer (Rigaku Corporation, Tokyo, Japan) fitted with CuK_α radiation (λ = 1.5406 Å). Fourier Transform Infrared Spectroscopy (FT/IR-4700, JASCO Analytical Instruments, Easton, PA, USA) in the spectral range of 500–4000 cm^{-1} was used to investigate bonding features. Moreover, the popular graphical software Origin Pro 9.0 (Origin Lab, Massachusetts, MA, USA) was used to plot the experimental data.

3. Results and Discussion

3.1. Characterization of the ZnO NPs in Aqueous Solution

The summary of the most important physicochemical properties of ZnO NPs is outlined in Table S1. Figure S1A shows the FT-IR spectrum of ZnO NPs, which shows a peak at approximately 554 cm^{-1}, attributable to the stretching vibration mode of Zn–O bond. The crystalline phase structure of commercial ZnO NPs is depicted in the XRD spectrum (Figure S1B). Diffraction peaks corresponding to ZnO with hexagonal-type structure in the XRD pattern were detected and compared with the JCPDS card No. 89-7102 (See Supplementary Material (SM) Section S3.1). The effect of sonication time (5–40 min) on solution turbidity and particle size distribution of ZnO NPs in nanopure water were investigated. As shown (Figure S2A), the best dispersion was obtained at 30-min sonication time, and no significant difference was observed above that time. Moreover, DLS measurement indicated that the majority of NPs were well dispersed in the water, and the HDD was in the range of 200–300 nm (Figure S2B), which was much larger than primary particle size (<50 nm). The change in particle sizes might be attributed to increases in Van der Waals (vdW) forces among the NPs; the surrounding solution would thus promote the formation of large aggregates [34]. The optical absorption spectrum of the different mass concentration of ZnO NPs (0–50 mg/L) in suspension was found to be proportional to the absorbed light (see Supplementary Material Section S3.1 and Figure S2C). The relative concentrations of C, N, H, and S in each organic ligand are shown in Table S2; C and S were shown to be the primary elements in HA, SA, and L-cys respectively. The relative C and S concentrations of HA, SA, and L-cys were (61.29%, 35.40% and 27.63%) and (0.63%, 0.49% and 24.68%) respectively.

The pH is a key environmental factor of the aquatic system, and fluctuations in pH directly affect the solubility, size, surface charge, and density of NPs in solution. The ZnO NP solubility, ζ-potential, and change in HDD at different pH values were investigated (Figure 1A). When the pH

value was between 2 to 3, the Zn^{2+} released from ZnO NPs (30 mg/L) was up to 21–24% of total Zn. However, ZnO NP solubility was reduced above pH 3, and only less than 0.8% of total Zn was measured at pH 7. Therefore, it indicated a negative correlation between solution pH and solubility of ZnO NPs (Figure 1A). High concentrations of H^+ in acidic conditions react with ZnO NPs and release a significant amount of Zn^{2+} ions. However, under weak acidic/alkaline conditions, a small amount of H^+ reacts with NPs, thus generating Zn $(OH)^+$ complexes [11]. Noyes-Whitney demonstrated that the dissolution rate might be related to the NPs surface area, since large size NPs aggregate faster, thus reducing the dissolution compared to smaller NPs [35]. As shown in Figure 1B, both ζ-potential and HDD of ZnO NPs were significantly affected by variation in the suspension pH. For instance, the ζ-potential was found positive at pH 4.5 to ~9.0, and remained negative at extremely acidic (2–4) and alkaline pH conditions (9.5–12). The point of zero charge pH_{zpc} of ZnO NPs was at 9.2, where the surface charge -2.7 ± 2.8 mV and HDD (above 800 ± 70 nm) were found to be higher than other pH values. The pH_{zpc} determined in the current study coincides with previous studies which report that the pH_{zpc} of ZnO NPs was between 8.7 to 9.4 [11,12,16]. At pH_{zpc}, NPs have negligible surface charge; due to weak repulsive interaction between NPs, each collision causes particle adherence and increases the HDD of particles [12,30]. These results are also consistent with previous reports [13,16], which affirm that ζ-potential is positive at pH values below the isoelectric point (IEP), and becomes negative at pH values above IEP. In our study, the ζ-potential remains positive (2 ± 0.3 to 15 ± 2.0 mV) for the pH values (4.5–8.5) prior to pH_{zpc}, and HDD ranges between 450 ± 20 to ~700 ± 55 nm. Particles with surface potentials below ±15 mV are considered unstable under electrostatic interaction, and tend to agglomerate, while NPs with high surface potential above ±30 mV are assumed to be stable [15].

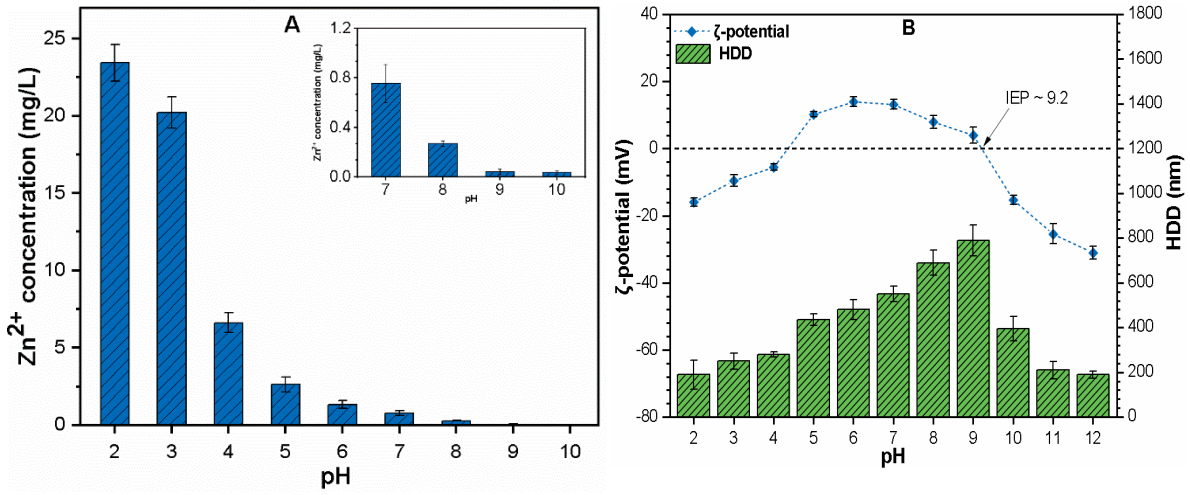

Figure 1. (**A**) Zn^{2+} released (mg/L); (**B**) ζ-potential and HDD profile of ZnO NPs (30 mg/L) suspension (mean ± SD, $n = 3$) as a function of varying pH. The inset in (Figure 1A) was the same enlarged figure from pH 7 to 10.

The ζ-potential of suspension in the pH range (9.5–12) was determined (-15 ± 1.2 to -32 ± 2.4 mV), which demonstrates highly stable colloids with smaller HDDs (190 ± 50 to 250 ± 35 nm). Such smaller sized particles at higher pH might be attributed to the deprotonation effect of pH, which increases the repulsive interaction between the highly-charged NPs [16]. Therefore, to minimize the dissolution effect, further experiments were carried out at circumneutral pH (pH 7.0).

3.2. Ligand Adsorption

The effect of organic ligand type and concentration on the surface charge and HDD of ZnO NPs were investigated at a neutral pH (Figure 2A). The results showed that ZnO NPs exhibit positive ζ-potential in the presence of low concentrations of organic ligand (1 mg/L HA, L-cys and 2.5 mg/L

SA), while the HDDs at these conditions were between 600–800 nm. The surface of ZnO NPs was positively charged at pH 7 (Figure 1B); however, the ζ-potential decreases with the addition of ligand, irrespective of type, and it approaches IEP at low concentration. This might be attributed to the charge neutralization which occurs when the electrical double layer (EDL) on the surface of NPs is effectively compressed due to the charge of adsorbed organic molecules, causing a reduction in electrostatic repulsions between ligand molecule and NPs [17,30]. The low amount of HA and L-cys significantly reduces surface charge because both contain –SH, carbonyl, carboxyl, aromatic, acetal, and hetero aliphatic groups, thus having a strong affinity to bind with the surfaces of the NPs [13,14]. In contrast, the surface charge of ZnO became negative upon further increasing the ligand concentration (5–100 mg/L), and the HDD of the particle ranged from 180–220 nm over the experimental trials. The coating effect of organic molecules such as HA, SA, and L-cysteine has been known to reverse the surface potential from positive to negative, and stabilize the ZnO NPs in solution [36]. Moreover, during the interaction, sulfur atoms present in L-cys may adsorb onto the NPs surface, leaving the free amino and carboxylic acid groups in the surface for conjugating biomolecules [18]. These results indicate that the interaction behavior between NPs and organic molecules depends on the properties of organic ligands. Moreover, variation in charge reversal might be related to specific adsorption mechanisms of the organic ligands on ZnO NPs. Therefore, adsorption kinetics and isotherms studies were conducted.

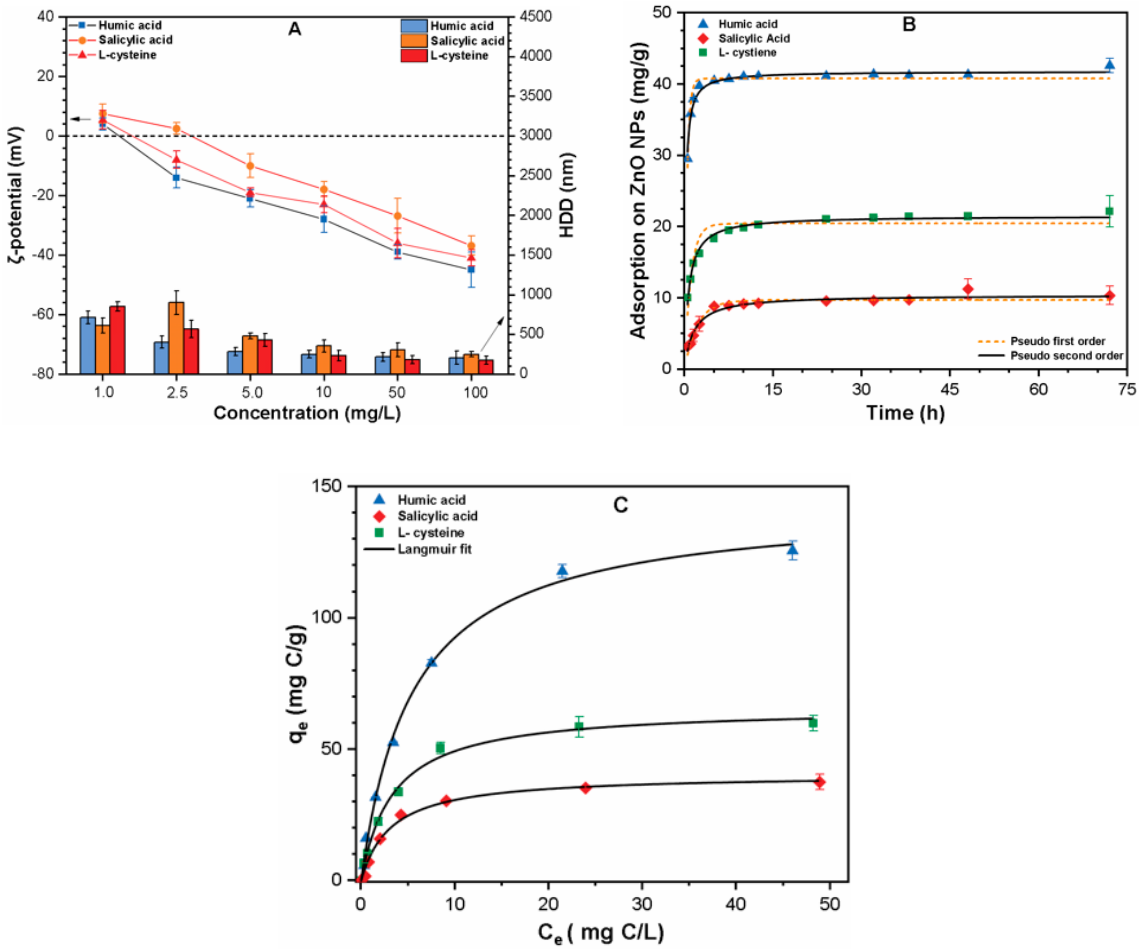

Figure 2. (**A**) The ζ-potential and HDD profile of ZnO NPs (30 mg/L) suspension at different concentration (1–100 mg/L) of organic ligands; (**B**) adsorption kinetics (10 mg/L of each organic ligand); (**C**) adsorption study (50 mg C/L of each organic ligand) at pH 7. The values are the mean of $n = 3$ (mean ± standard deviation).

Figure 2B shows that ligands such as HA, SA, and L-cys (10 mg/L) demonstrate different degrees of adsorption onto ZnO NPs (30 mg/L) with time. The adsorption of HA, SA, and L-cys onto ZnO NP surfaces was rapid, and reached about 92%, 79%, and 84% of their adsorptions respectively after 7.5 h. However, it took an additional 16.0 h to reach 97.5% of its maximum adsorption capacity, which indicates a rapid initial adsorption followed by slow adsorption, and then a leveling off. This might be attributed to more interstices between NPs that reduced the ligand molecules binding to the active surface sites of ZnO NPs [37,38]. Moreover, at the initial step, the ligand molecules self-aggregated by π-π stacking interactions, which played an essential role in the second step in aromatic rings adsorption on the surface. The carboxyl group present in the ligand might bind to the Zn^{2+} of the NPs surface to form an inner-sphere complex by replacing the previous adsorbed hydroxyl groups [13,33]. These results are consistent with previous studies which report that 24 h is sufficient for the adsorption of natural organic matter (NOM) on ZnO, TiO_2, and Al_2O_3 NPs to attain equilibrium [39–41] The result demonstrates that adsorption of HA was more significant and faster than that of SA and L-cys, based on rate constant (k), as well as adsorption rates (Table 2). This was attributed mainly to the higher content of phenolic, aliphatic species, and lower contents of carbonyl, carboxyl species in the hydrophobic ligand, as compared to the hydrophilic. These results agreed with a previous observation [18,36] that hydrophobic ligands have a higher affinity to AgO_2 and TiO_2 NPs due to their lower solubility and HMW. It is noteworthy that little adsorption of organic ligands was observed after 24 h, which might be ascribed to some other interaction between ligand molecules and NPs. Therefore, due to the heterogeneity of organic ligands, the interaction phenomena between the ZnO NPs and ligand is much more complex. Furthermore, the experimental data fitted better with the Pseudo-second order (PSO) model for its high correlation coefficients than the Pseudo-first order (PFO) model (Table 2). This suggested that the attachment of organic ligands onto ZnO NPs was proceeded by a chemical adsorption phenomenon.

Table 2. Kinetic parameters used to describe the adsorption of organic ligands on ZnO NPs.

Adsorbate	Pseudo-First Order (PFO)			Pseudo-Second Order (PSO)		
	q_e (mg/g)	k_1 (1/h)	R^2	q_e (mg/g)	k_2 (g/mg/h)	R^2
HA	40.91	5.405	0.917	41.78	0.1385	0.976
SA	9.822	1.042	0.937	10.44	0.0632	0.972
L-cys	20.46	2.146	0.863	21.52	0.0681	0.986

To further elucidate the adsorption phenomenon, the isotherm study was conducted under varying organic ligands concentration (0.1–50 mg C/L) with ZnO NPs concentration (30 mg/L), as shown in Figure 2C. As expected, the hydrophobic ligand HA showed a strong adsorption ability compared to both hydrophilic ligands. The HA isotherm reached a plateau at a concentration of more than 20 mg C/L, indicating almost complete surface coverage at higher concentrations (Figure 2B). Moreover, the adsorption isotherms for binding organic ligands on ZnO NPs were further fitted with Langmuir and Freundlich models. Results showed that adsorption on ZnO NPs was better fitted by the Langmuir model, with adsorption maxima of 143.35, 66.05 and 40.47 mg/g for HA, SA, and L-cys respectively (Figure 1C and Table 3). This observation indicated the high adsorption capacity of hydrophobic ligands in comparison to hydrophilic ones. Similar phenomena have been observed in previous studies [32,33], where preferential adsorption of HMW hydrophobic ligands was observed on Fe_3O_4, and TiO_2 NPs, thus providing a more thermodynamically-favorable surface. The strong sorption capacity of L-cys has been previously described [13,34], where adsorption of cysteine onto CuO and Ag NPs results in the formation of Cu (II)–S and Ag (I)–S bonds. Our results showed that organic ligands with HMW adsorbed to ZnO NPs more effectively due to the higher level of adsorptive interaction of organic molecules with NP surfaces; see Figure 2B. The present results also imply that the aromatic content and hydrophobicity of organic molecules could be useful for evaluating the level of ligand adsorption onto ZnO NPs. Nevertheless, the finding in Table 3 suggests that the adsorption

capacity is closely related to the aromatic group content in the organic substance. For instance, HA with a higher degree of substitution of aromatic rings, by groups such as phenolic or hydroxyl, may be linked to greater adsorption capacities. These results are consistent with past studies which reported that the attractive interaction between chemical compounds containing the aromatic moiety and carbon nanotubes (CNT) was driven mainly by π-π interaction [33]. In general, such observations suggested the monolayer adsorption of organic ligands was formed on ZnO NPs.

Table 3. Langmuir and Freundlich fitting for HA, SA and L-cys adsorption on ZnO NPs.

Ligand	Langmuir Fitting			Freundlich Fitting		
	K_L (L/mg)	q_m (mg/g)	R^2	K_F (mg/g) (L/mg)$^{\frac{1}{n}}$	n	R^2
HA	0.18 ± 0.01	143.37 ± 3.30	0.996	31.60 ± 5.51	2.58 ± 0.36	0.939
SA	0.31 ± 0.04	40.47 ± 1.48	0.988	12.37 ± 2.49	3.18 ± 0.66	0.877
L-cys	0.29 ± 0.02	66.05 ± 1.77	0.994	19.96 ± 3.48	3.17 ± 0.57	0.905

3.3. Influence of Synthetic Waters on the Behavior of ZnO NPs

3.3.1. ζ-Potential and Particle Size of ZnO NPs

The water characteristics not only influence the NP distributions, but may also alter the transport behavior of NPs in the environment. Figure 3 shows the ζ-potential and HDD of ZnO NPs in prepared synthetic waters (S1–S8). It can be observed that the ζ-potential and HDD of ZnO NPs were jointly affected in synthetic waters due to the different DOC types and concentration. The ζ-potential and HDD values vary, ranging between +4.7 ± 2.0 to −38.3 ± 5.0 and 690 ± 90 to 220 ± 26 respectively in all studied waters.

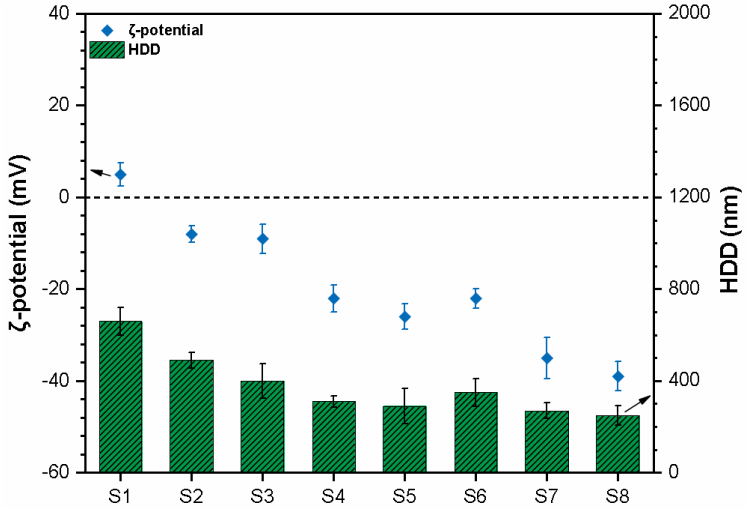

Figure 3. Corresponding ζ-potential and HDD profile of ZnO NPs (30 mg/L) dispersed in synthetic waters (S1–S8) at pH 7.

These results suggest that organic substances decrease the surface potential by imparting a negative charge onto the NP surface, thus stabilizing the ZnO NPs in suspension [42]. Additionally, the ligand exchange might be responsible for the increase in negative surface potential due to the relatively high binding affinity of metal ions with a carboxyl group [15]. A sharp increase in HDD of ZnO NPs, i.e., 520–690 nm, was observed in S1, S2, and S3 waters, whereas, the ζ-potential value closer to IEP in these waters suggested poor stability of ZnO NPs. This might be attributed to the adsorption of functional groups such as carboxylic and amine onto the NPs surface through electrostatic attraction, which tends to enhance the HDD of particles [17,20]. The moderately high DOC concentration in hydrophobic/hydrophilic waters (S4–S8) reverses the surface charge with a relatively small difference in

HDD (Figure 3). According to previous studies [26,36], high DOC concentration increases the surface coating and coverage onto the NPs, which decreases the total surface charge (more negative) and enhances the steric, as well as electrostatic, stabilizing effect. In general, hydrophilic, LMW organic ligands with carboxylic groups bonded on aromatic rings form loop or tail structure that extend away, thus affecting ZnO NP suspensions [17].

3.3.2. Dissolution and Aggregation of ZnO NPs

The release of NPs into the aquatic environment increases their bioavailability to organisms. Thus, processes like aggregation and sedimentation might reduce their dissolution as well as associated potential risks. Considering the dissolution of ZnO NPs with time, the release of Zn^{2+} ions and the change in the suspension pH were monitored for each synthetic water. In the absence of ligands, the concentration of Zn^{2+} was only 0.8 mg/L at pH 7 (Figure 1A), whereas the Zn^{2+} ion concentration increased gradually as a function of increasing DOC concentration in synthetic waters. As shown in Table S3, the highest Zn^{2+} concentration was found to be 2.26 ± 0.05 and 2.54 ± 0.02 mg/L in S7 and S8 respectively. It is well known that HA promotes ZnO NP dissolution via complexation and coordination with metal ions. It was reported that complexing ligands could adsorb on the majority of flat terraces, as well as polarize and weaken the metal–oxygen bonds of the lattice surface. Thus, in the presence of such ligands, additional dissolution hot spots are created on the terraces other than the edges and links, leading to the dissolution of nanoscale material [16]. The L-cys may interact with NPs via one of its functional groups, thus forming polymers via bridging thiolate sulfur [18,34]. In contrast, the lower dissolution in remaining waters might be attributed to the surface adsorption of ligands onto ZnO NPs. Moreover, coated NPs may behave as a competitive sink to form oxidation compounds, thus inhibiting the oxidation of NPs [40]. Additionally, it is postulated that the reactive surface areas of the NPs exposed to the solution is reduced due to aggregation, and the solution properties within the aggregates are different from the bulk. Therefore, aggregation plays a significant role in nanoparticle dissolution in an aqueous system. The results showed that the impact of dissolution during the 24 h experiments was considered to be minor on the ZnO NPs suspension.

The results of the sedimentation and aggregation behavior of ZnO (30 mg/L) NPs dispersed in control water, and synthetic waters are shown in Figure 4A,B. It can be observed in (Figure 4A inset) that a 50% loss of absorbance within 2 h occurred for ZnO NPs suspended in control and hydrophilic (S1, S2, and S3) waters. The surface charge of ZnO NPs in these waters were close to IEP (Figure 3); therefore, the enhanced aggregation and sedimentation rate of NPs was majorly due to charge neutralization between the positively charged NPs and the negatively charged ligands molecules (Figure 4A,B) [15]. Electrostatic interactions between carboxylic groups (COO^-) of ligands and NPs at/near IEP increase due to less DOC being adsorbed on the NP surfaces, contributing to the aggregation of NPs in solution [14,38]. However, only a 25–35% loss of absorbance within the first two hours and milder aggregation curve in S4 and S6 was observed (Figure 4A). The grafting of organic matter onto the surface of NPs altered the surface charges and increased electrostatic repulsion between NPs and organic media [43]. Similar results were observed in Section 3.2 of this study, where negatively charged carboxylate, phenolic, and thiol functional groups reverse the ZnO NPs surface charge from positive to negative (Figure 2A). In contrast, the high L-cys concentration in hydrophilic water (S7) significantly impeded the aggregation and sedimentation process of ZnO NPs (Figure 4A,B). Such discrepant aggregation behavior was consistent with previous reports that the disulfide groups in L-cys can sorb on the surface of NPs, thereby inverting the surface potential of NPs and keeping them suspended in solution [32]. As shown (Figure 4A,B), the hydrophobic waters S5 and S8 present the slowest aggregation and sedimentation rates (less than 0.02 h^{-1}) compared to the (0.02–0.07 h^{-1}) hydrophilic waters. The organic anions in HA enhance the negative charge density adjacent to the NPs surface and cause a shift in the position of the shear plane further away from the surface, resulting in a decrease of ζ-potential of NPs, as well as antagonizing the aggregation-promoting effect from the electrolytes [44]. Moreover, the MW of organic ligands significantly affects the thickness of the adsorption layer, thereby

affecting particle interactions during the aggregation process. This result agreed with those of a previous study [36].

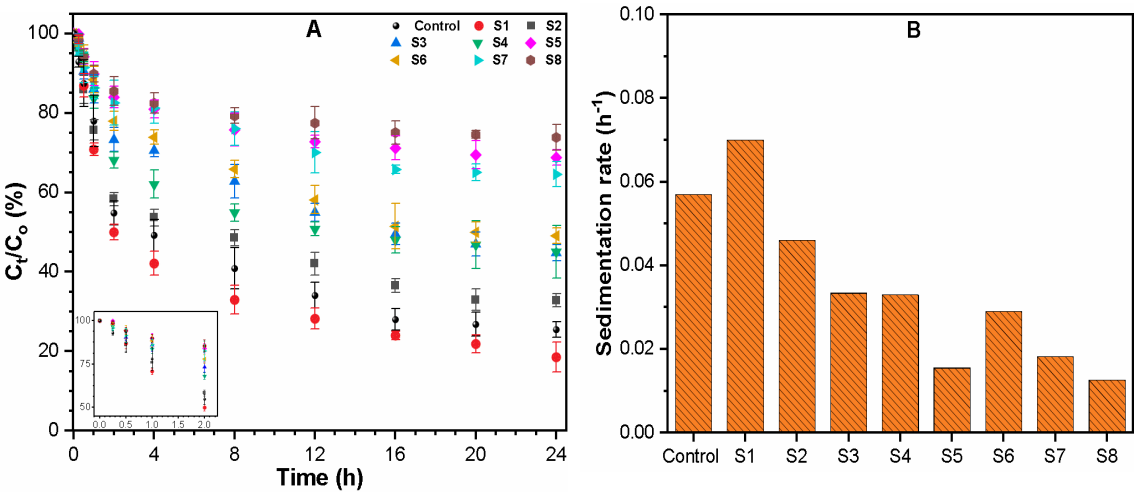

Figure 4. (**A**) Aggregation kinetic and; (**B**) sedimentation rates K (h^{-1}) of ZnO NPs (30 mg/L) suspension in various synthetic waters after 24 h respectively.

To further understand the effect of NP concentration on aggregation geometry, sedimentation experiments at low (10 mg/L) and high (50 mg/L) concentrations of ZnO NPs were conducted in selected (S1, S4, S5, and S8) waters. For a lower NP concentration (10 mg/L), a slight decrease in the NP aggregation rate was observed (Figure S3). However, a higher NP concentration (50 mg/L) slightly enhanced the aggregation and sedimentation rate (Figure 5A,B). This result is consistent with previous studies, which shows that at higher NP concentrations, collision probability and frequency increases among surrounding particles, thereby enhancing the NP count [45]. However, irrespective of NP concentration, the aggregation behavior was found to be similar in synthetic waters.

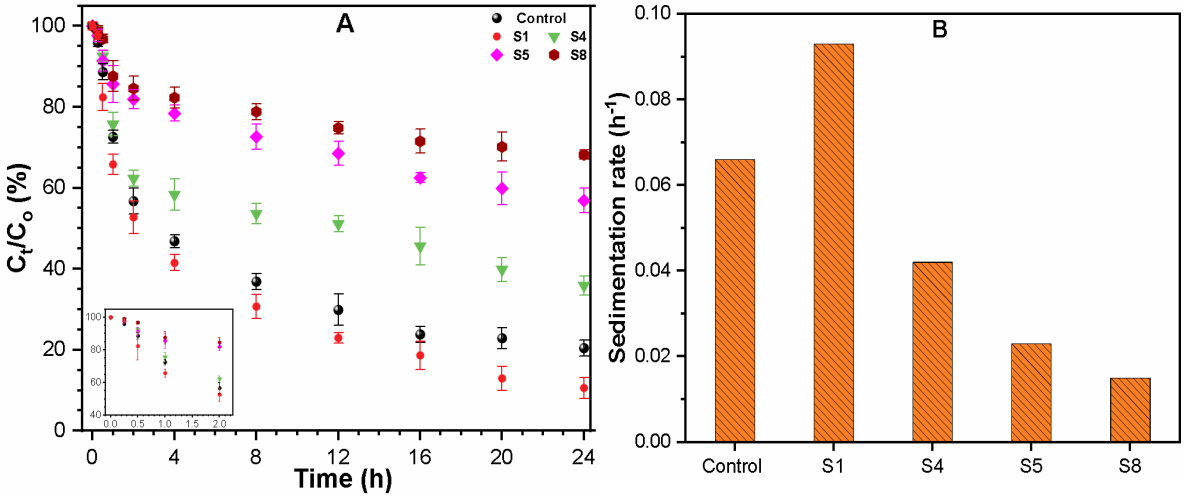

Figure 5. (**A**) Aggregation kinetic and; (**B**) sedimentation rates K (h^{-1}) of ZnO NPs (50 mg/L) suspension in selected synthetic waters after 24 h respectively.

Fast aggregation and higher sedimentation rates of ZnO NPs were observed in waters containing hydrophilic ligands S1 and S2 (0.092 and 0.04 h^{-1}), as compared to waters with hydrophobic ligands S5 and S8 (0.021 and 0.014 h^{-1}). The results of the above study demonstrated that the characteristics of organic ligands remarkably affect the aggregation and sedimentation behavior of ZnO NPs.

Therefore, the prolonged stability of ZnO NPs might cause a serious concern, i.e., the NPs could be transported into the aquatic environments and may endanger aquatic organisms.

3.3.3. Removal of ZnO NPs and Zn^{2+}

Figure 6 shows the removal of ZnO NPs, Zn^{2+}, and the corresponding ζ-potential values of synthetic waters (S1 to S8) after coagulation with various FC dosages. Under control conditions, around 50–75% ZnO NP removal was observed in hydrophilic waters (S1, S2, S3, S4, S6, and S7), as compared to 20–30% in hydrophobic water (S5 and S8). These results are in good agreement with the result of a previous study [40], which reported that large NPs with organic matter auto-precipitate in the absence of coagulant. Another possible reason for the high removal rates in hydrophilic waters may be the presence of divalent metal cations Ca^{2+} which effectively compresses the diffuse layer (DL) associated with the particles, and weakens interparticle repulsion, thus promoting flocculation [12]. However, removal efficiencies of Zn^{2+} were quite low (<20%), regardless of water type at control conditions.

The addition of FC dose increases the removal efficiencies of both ZnO NPs and Zn^{2+} in all the waters. The presence of FC results in ampler NP flocs formation, until it reaches the effective coagulation zone (ECR), which is called a plateau, i.e., where ~95% of removal is achieved [46]. The ECR for hydrophilic waters varies between 0.025–0.125 mM for S1, S2 with optimum doses (ODs) of 0.025 and 0.05 mM (Figure 6A,B), between 0.05–0.175 mM for S3, S4 with OD 0.10 mM each (Figure 6C,D), between 0.10–0.25 mM for S6, S7 with OD 0.15 and 0.175 mM (Figure 6F,G) respectively. The hydrophobic waters S5 and S8 present higher ECR zones between 0.15–0.40 mM, with ODs at 0.225 and 0.35 mM (Figure 6E,H) respectively. This result indicated that NP size plays an important role in determining the ECR; thus, the smaller the NPs size, the broader the ECR zone [47]. In our study, ZnO NPs (Figure 3) shows large size aggregates in hydrophilic waters than hydrophobic waters, while the ECR zone followed the reverse phenomena. These results also show that NP removal depends upon the character of organic ligand present in source water and dosage of coagulant during the coagulation process. For instance, the hydrophobic waters (S5 and S8) require a higher FC dosage to achieve the similar ZnO NPs and Zn^{2+} removal compared to hydrophilic waters. A similar observation has been made in previous studies, where water with higher UV_{254} values require more coagulant dose to achieve a higher removal rate [26]. After the ECR zone, the excess of a coagulant promotes the re-stabilization of the ZnO NPs, and consequently decreases the rate of NP removal. This phenomenon could be attributed to charge inversion and restabilization of coagulated colloids due to polyelectrolytes oversaturation [41,43].

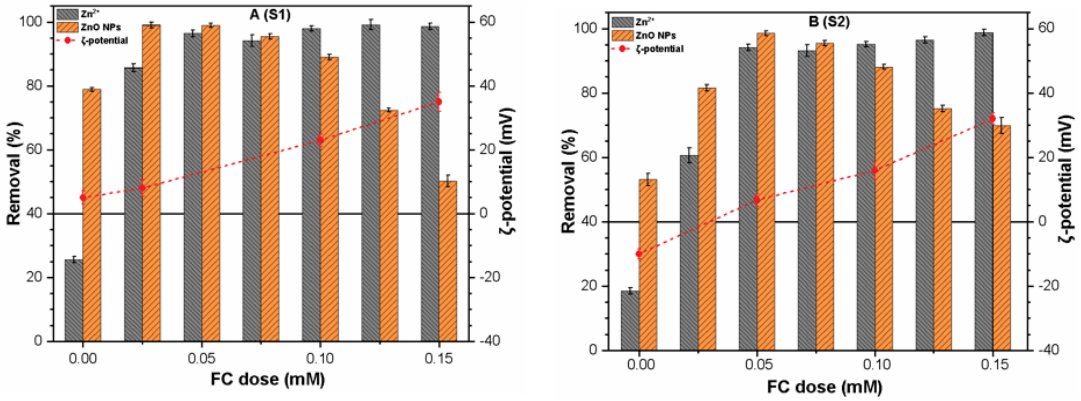

Figure 6. *Cont.*

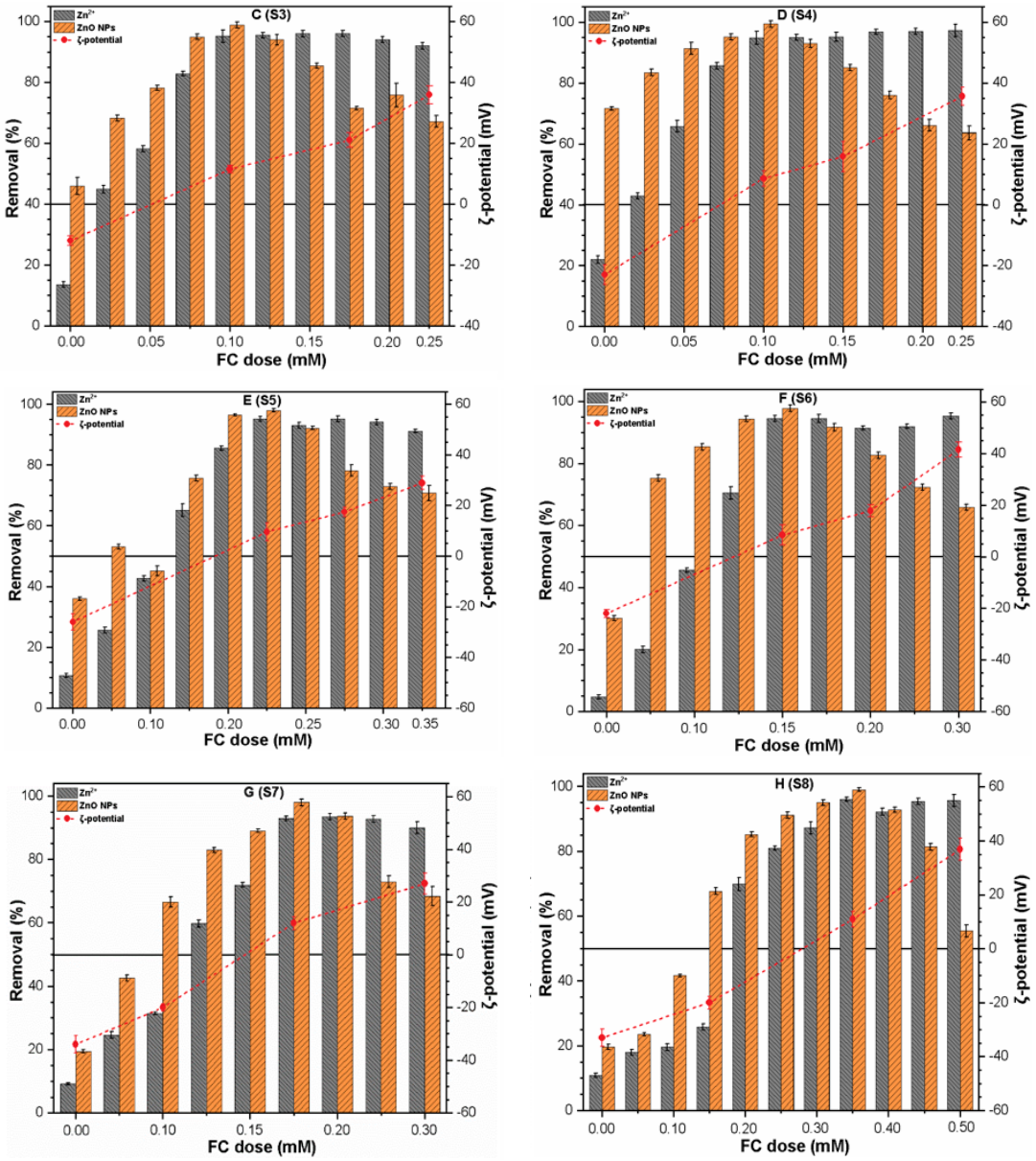

Figure 6. Removal of ZnO NPs and Zn^{2+} from synthetics waters (S1–S8) as a function of coagulant dose with corresponding ζ-potential.

In all studied waters, relatively less Zn^{2+} removal was achieved at low FC dosage, probably due to less available Fe attachment sites. However, up to 90–98%, Zn^{2+} removal was observed at OD irrespective of water type. The effect of FC on Zn^{2+} removal was consistent with previous literature, which suggests that the presence of heavy metals in cationic form might be associated with the precipitate matrix particle via mechanisms known as occlusion [48]. Furthermore, ZnO NP removal rates increase with FC dosage, until reaching the OD in the ECR zone; they decrease at higher FC dosages. At a low FC dose, the flocs did not form because the coagulant was not adequate to compress the EDL of the colloid particles or to bind the colloid particles to form interparticle bridging [29]. The ZnO NPs in control samples were negatively charged (-10 ± 1.3 and -40 ± 2.1) in all waters except S1, as shown in (Figures 3 and 6). The addition of FC coagulant induces the destabilization of ZnO NPs, due to the neutralization of the NPs negative surface charges by positively charged hydrolyzed Fe^{3+} species in suspension. Consequently, the Fe hydrolysis product strongly adsorbs onto the NPs surface, and ζ-potential increases and approaches IEP. This result may be explained by the fact that at OD, NPs are completely destabilized, the surface charge is practically neutral, and colloids

flocculate owing to the decrease of the electrostatic repulsion between surrounding NPs (Figure 6). Similar results were observed in the previous study, which reported that NPs could be destabilized and effectively removed in the range of ζ-potential between −20 and + 20 mV [19]. The small size NPs in the stable waters (S5, S7, and S8) present more negative charge compared to the large particle (S1–S4 and S6), as shown in Figure 3. Hence, such stable suspensions will consume more FC to neutralize their charges and induce them to destabilize in the process of coagulation. The HA and L-cys may bind to the NPs surface and act as an electrostatic stabilizer, thus enhancing the stability, as observed from the smaller particle size of ZnO NPs in these waters. However, at OD, the enmeshment of the coagulants was much stronger than the repulsive force between ZnO NPs, and played a dominant role in removing NPs from the water. As shown (Figure 6A–H), the increase of coagulant dose shifts the ζ-potential to higher positive values more than +20 mV. Thus, restabilization occurs due to the highly positive surface of ZnO NPs. It is evident that restabilization decreases the NP removal rate. The colloidal system becomes stabilized, resulting in lower removal efficiency of ZnO NPs (Figure 6). The result of the measured pH of suspension before and after the coagulation indicated no significant change. However, a slight decrease in the pH of hydrophobic waters was observed. As previously reported [20,44], when aqueous Fe(III) salt is added to water, it will dissociate to respective trivalent ions, i.e., Fe^{3+} in suspension with strong ability of hydration to form hydroxo complexes. This reaction results in the formation of H^+ ions in such suspensions, which will lower pH values. The results of all eight synthetic waters revealed the clear dependency of the ZnO NPs and Zn^{2+} removal on source water characteristics, specifically, ligand type and applied coagulant dosage, as well as demand.

3.3.4. Removal of DOC and UV_{254}

Different organic matters are present in subsurface and groundwater environments, and may adsorb on the surface of NPs and affect the overall colloidal stability. The removal efficiencies of organic substance-related parameters, DOC and UV_{254}, are presented in Figure 7. The results show that at/near the ECR zone, the highest removal of DOC and UV_{254}, 90% in hydrophobic waters (S5, S8, Figure 7E,H) and lowest 23% in hydrophilic waters (S1–S4, S6, and S7, Figure 7A–D,F,G) was achieved. This indicated that the hydrophobic fraction of organic ligand could be removed more efficiently than the hydrophilic fraction. These findings are consistent with previous reports [28,29], and could be explained as follows: in waters with SUVA > 4.0 L/(m mg), ligands principally control the coagulation process, and more than 50% DOC removal is achieved because suspension contains humic substances with high hydrophobicity and HMW aromatic compounds. Similarly, waters with (SUVA < 2 L/(m mg)), organic ligands have little influence on coagulation, and less than 25% DOC is removed, since they are composed of non-humic, hydrophilic and LMW compounds. Interestingly, the UV_{254} is more reduced than DOC, irrespective of water type, which suggests that aromatic matters are removed more efficiently than other organic ligands fractions. This behavior can be attributed to that hydrophobic fraction which has a low IEP, due to the abundance of carboxylic and phenolic groups, resulting in higher coverage of NPs with negative charges, as observed in Figure 3 and reported in a previous study [49]. The hydrophobic waters contain higher anionic binding sites, resulting in effective charge neutralization with cationic Fe hydrolysis products compared to hydrophilic waters at the appropriate dosage [50]. In addition, the Fe hydrolysis with different polymerization degrees and amorphous hydroxide solids may form insoluble complexes with HA, which could efficiently remove from the system [29,30]. Further analysis of coagulation performance revealed a clear relationship between ζ-potential and residual DOC in studied waters. It has been reported that there is an operational ζ-potential window (−10 and +3 mV), where most of the colloids are optimized and stable can be removed [51]. However, the removal of hydrophobic fractions strongly depends upon the magnitude of the coagulation ζ-potential. The DOC and UV_{254} results of hydrophobic waters at ζ-potential around +10 mV show high removal (>90%), but slightly decrease at ζ-potential (~±30 mV) (Figure 7E,H). In addition, the DOC and UV_{254} removal in hydrophilic waters were between (1 to 25%) and (10 to 60%) respectively (Figure 7A–D,F,G).

This might be attributed to the presence of weaker acidic groups and LMW compounds in hydrophilic waters, thus hindering the competitive interactions between coagulants and ligands molecules [20,47]. In general, the removal behavior of both DOC and UV_{254} follow the removal pattern of ZnO NPs, where higher removal efficiency was observed at OD of coagulants in all waters. This suggests that ligand type (hydrophobic/hydrophilic) is likely to influence on removal efficiency and coagulant dosage during the water treatment process. These results are in good agreement with previous studies which have shown the high removal of hydrophobic organic fraction from water using coagulation [52,53]. The hydrophilic LMW (SA and L-cys) fraction likely influences the achievable residual post-treatment, due to its poor removal during conventional coagulation. The presence of zinc-based NPs might also contribute to the enhanced removal of DOC, UV_{254} in hydrophobic waters. A recent study showed the adsorbent effectiveness of zinc-based NPs at removing organic ligands from water [54]. Thus, the coagulation of ZnO NPs associated with the FC may have a positive effect on overall removal. However, further work is needed to confirm this interpretation. Based on our finding, ligand type appears to be a crucial factor in influencing the treatability, and should be included in any mechanistic approach to drinking water treatment.

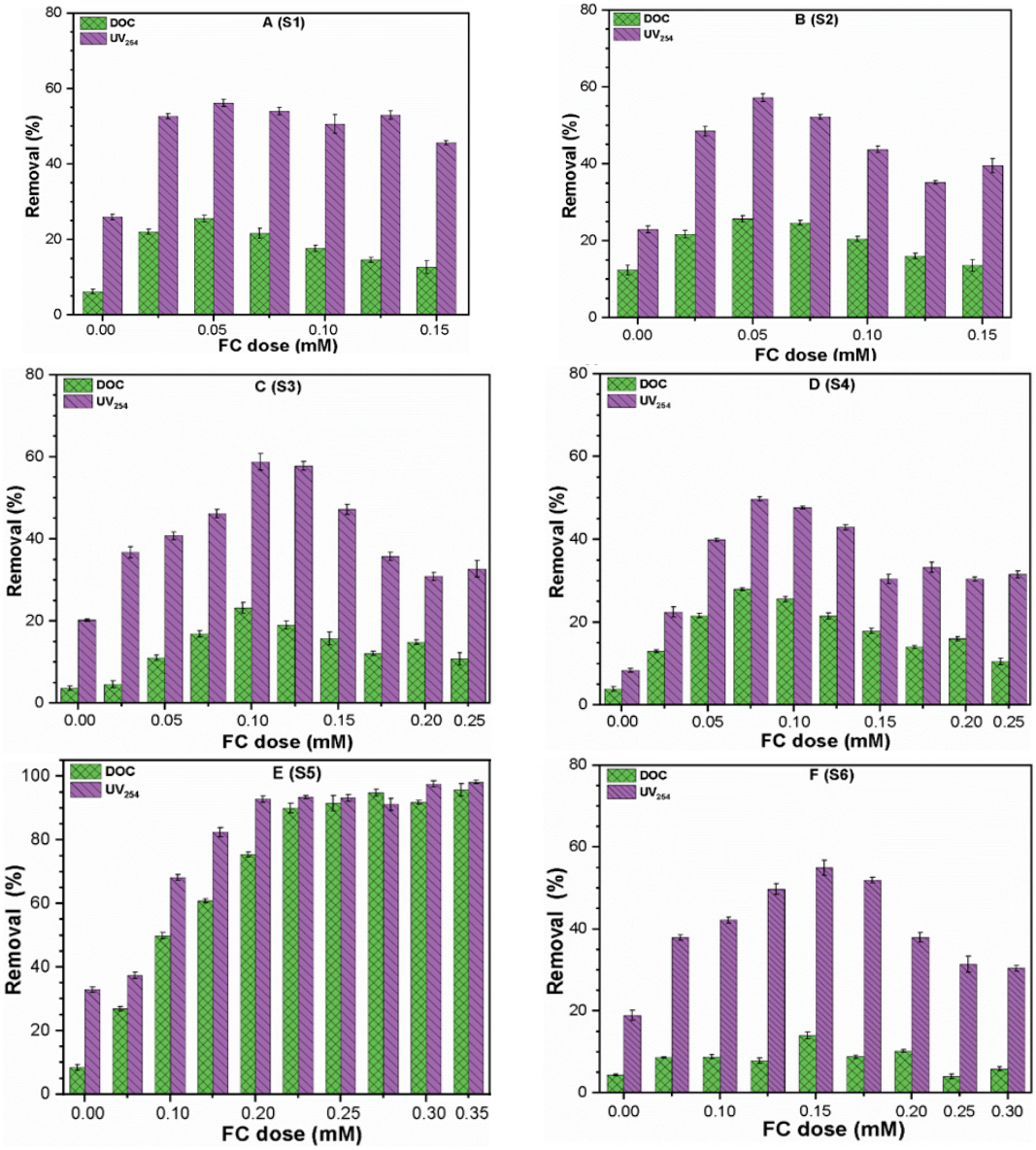

Figure 7. *Cont.*

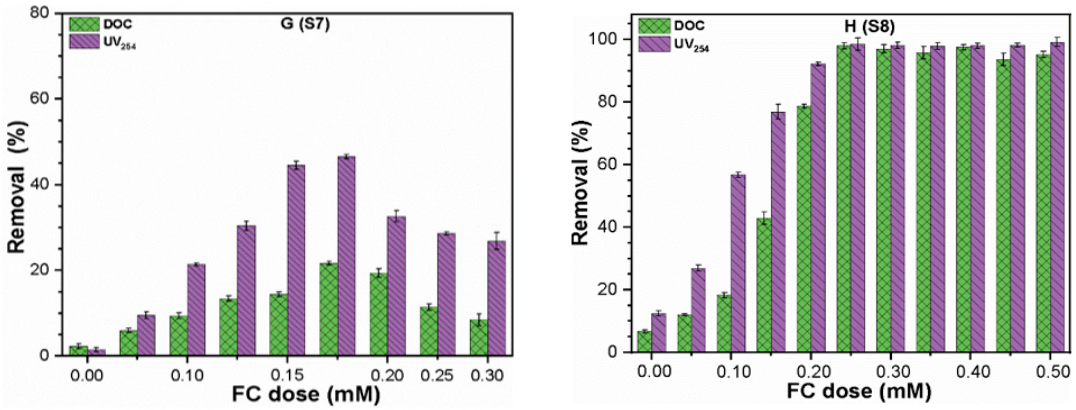

Figure 7. Removal of DOC, UV_{254} from eight synthetic waters (A-H) with different dosage of FC coagulant.

3.3.5. Characteristics of Flocs

The FT-IR analysis of pristine organic ligands and precipitates of selected waters (S6, S7, and S8) were recorded to expound the bond formation, as well as possible coagulation mechanisms, as presented in Figure 8. As shown in Figure 8A, the peaks around 3653, 2972 cm^{-1} and 2887 cm^{-1} correspond to OH, asymmetric and symmetric stretching vibrations of aliphatic C–H and $C–H_2$ moiety [55]. The peak at 2082 cm^{-1} and a weak band at 2548 cm^{-1} were attributed to the stretching vibrations of the N–H and S–H group respectively [34]. Furthermore, the peaks observed at 1609 and 1653 cm^{-1} were assigned to the asymmetric and symmetric stretching vibration of C=O (COO^{-}) [56]. The peaks at 1382, 1398, and 1263 cm^{-1} correspond to the symmetric stretching vibration of CH_3, COO^{-} and C–O anti-symmetric stretching [57]. Furthermore, some peaks around 1295, 1263, 1147, 1041, 1069 and 954 cm^{-1} may be ascribed to the stretching vibration of S=O, C–OH (phenolic), C–O, C–O–C, carbohydrates and carboxylic acid groups [17,24]. The peak at 739 cm^{-1} corresponds to the stretching of the F–O bond [58].

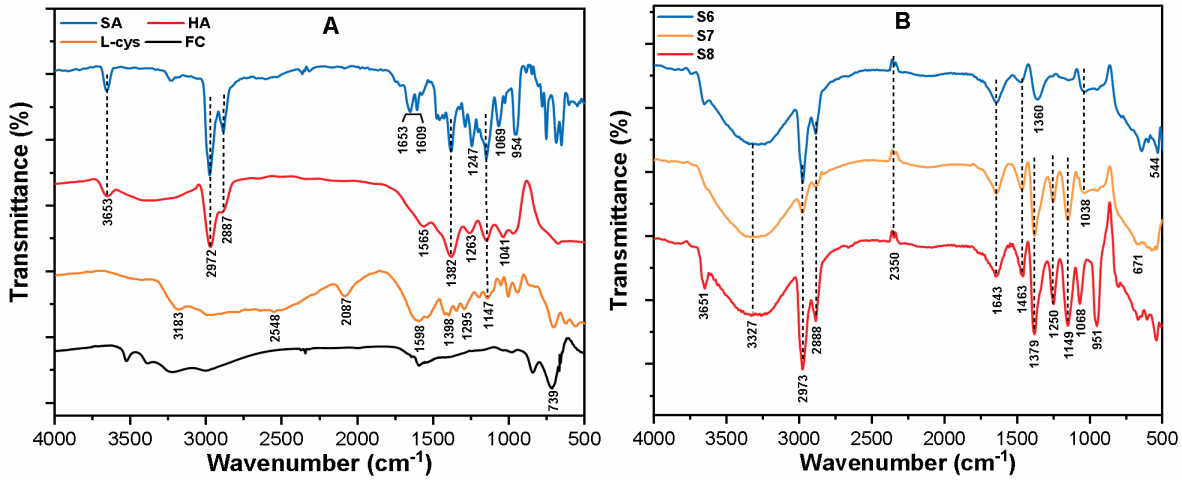

Figure 8. FT-IR spectra of (**A**) pristine organic ligands (HA, SA, L-cys, and FC); (**B**) synthetic water (S6, S7, and S8) flocs in obtained at OD in coagulation process.

Figure 8B shows the IR spectra of synthetic waters (S6, S7, and S8) flocs by FC. The broad peak in all flocs at 3327 cm^{-1} is due to the polar interaction of Fe ions and their hydrolyzed products, which tend to form complexes with metal ions [59]. The disappearance of S–H band at 2548 cm^{-1} in S7 indicates the formation of covalent bonds between thiols and Zn^{2+} onto the NPs surface [60]. The shift in the peak of C=O from 1263 to 1250 cm^{-1} further clarified that carboxyl, hydroxyl, and aromatic ester groups could be involved in complex coordination with metal ions during adsorption of the target

pollutants [24,25]. The peak at 1041 cm^{-1} shifted to a higher frequency at 1068 cm^{-1} with increased intensity due to Fe–O/Zn–O stretching vibration. Moreover, the bending vibration of Zn–O–Fe and Fe–O–Zn/Fe–OH–Zn bonds were found at 951 and 671 cm^{-1} [61–64]. Thus, the significant shifts, as well as the disappearance of distinct peaks in the flocs, supported the complex reaction of metal ions and composite contaminants with FC. Therefore, it can be inferred from the high removal efficiency and FT-IR spectra, that the principal mechanism for ZnO NPs and Zn^{2+} with organic ligand might be the combination of charge neutralization (for colloids), entrapment, complexation, and ligand exchange adsorption. This mechanism is consistent with previous research [19–24] working on the removal of other ENPs by coagulation. However, because of the variable composition of the organic substances, the removal mechanism might vary according to the specific type of organic ligands molecules present in water.

3.4. Environmental Significance

The incorporation of ZnO NPs into a wide variety of consumer products has led to concerns about their unintended release to drinking water sources. This study provides some insight into the aggregation, dissolution, and removal behavior of ZnO NPs in environmental water, which could limit the release of metal ions and lead to the removal of NPs to reduce potential risk. Our results highlight that the sorption of organic ligands onto the NP surfaces sterically stabilized the NPs, as well as enhancing their solubility. Thus, simultaneous transformations of ZnO NPs into Zn^{2+} could alter the bioavailability of the NPs to exposed organisms. However, the rate of dissolution depends upon the aggregation conditions of the NPs and surface modifications caused by sorption of ligand molecules. It appears that the environmental fate of ZnO NPs would be largely influenced by the type and concentration of organic ligands, as well as the solution chemistry. Other water quality parameters such as metal cations, temperature, as well as the presence of inorganic compounds, which were not examined in this study, might play a critical role in determining the extent of ZnO NPs and organic ligand interactions. Herein, we demonstrated that the coagulation process could not only remove ZnO NPs, but also limit the Zn^{2+} to a low level in the potable water. This study underscores the importance of understanding the impact of the various organic ligands on the fate of NPs and their persistence in the natural water environment.

4. Conclusions

In this study, we systematically investigated the effect of organic ligand types such as hydrophobic/hydrophilic, and their effects on ZnO NPs stability and removal by FC coagulant from synthetic waters. Our results demonstrated that hydrophobic ligands, e.g. HA, significantly reduce the HDD and ζ-potential compared to hydrophilic ligands like SA and L-cys due to their strong sorption capacity. The isotherm study revealed that ligands develop monolayers by binding to Zn^{2+} on the surface of ZnO NPs via ligand exchange and H-bonding. The low DOC concertation enhanced the aggregation kinetics of ZnO NPs due to charge neutralization, while high concentrations impeded NP aggregation, likely due to steric effect induced by the adsorbed organic molecules. The results showed that FC coagulation could effectively remove ZnO NPs, Zn^{2+} and ligand composite pollutants. At the ECR zone, the removal efficiencies of ZnO NPs and Zn^{2+} were more than 95%, irrespective of water type. However, after the ECR zone, the removal rate of NPs declined to 60% due to the restabilization of precipitated NPs. A higher ZnO NP removal rate was obtained at lower FC dosage in hydrophilic waters, as compared to hydrophobic waters; this indicated that the organic ligand type played a predominant role in determining ECR during coagulation. The highest reduction <93% in DOC and UV_{254nm} were obtained in the hydrophobic water in comparison to <23% in hydrophilic waters. The FT-IR analysis of flocs revealed that mechanisms such as charge neutralization, complexation, entrapment in precipitates and bridging effect might be involved in the removal of ZnO NP composite contaminants by FC coagulation. These findings provide some insight that the type of organic ligand

may influence the fate, transport, and coagulation performance of released ENPs in drinking water treatment processes.

Supplementary Materials: The following are available online at http://www.mdpi.com/2227-9717/6/9/170/s1, Figure S1: (A) FT-IR spectra and; (B) XRD pattern of commercial ZnO NPs powder; Table S1: ZnO NPs physicochemical properties; Table S2: Natural and synthetic water characteristics; Figure S2: (A) Effects of sonication time (5–40 min) on the dispersion turbidity of (30 mg/L) ZnO NPs; (B) Hydrodynamic size distribution of ZnO NPs in water after 30 min sonication; (C) UV-Vis spectra of ZnO NPs at a various initial concentration (0–50 mg/L); Table S2: The Relative concentration of C, N, H and S in various organic ligands;; Table S3: The Dissolution of ZnO NPs and the change of suspension pH in synthetic waters; Figure S3: Aggregation of ZnO NPs (10 mg/L) in selected synthetic waters; Figure S4: The fit of aggregation data to the stokes equation. Exponential model for ZnO NPs (30 mg/L) at pH 7 in nanopure water.

Author Contributions: R.K. and I.T.Y. designed the study; R.K., M.A.I. performed the experiment and analyzed the data; S.Z.Z., D.R.P., S.S., S.K. and M.A. provided critical feedback and helped shape the research; R.K. wrote final version of the manuscript.

Acknowledgments: This work was supported by the BK21 plus program through the National Research Foundation of Korea(NRF) funded by the Ministry of Education of Korea (Grant No. 22A20152613545).

Conflicts of Interest: The authors declare no conflict of interest.

References

1. Keller, A.A.; Vosti, W.; Wang, H.; Lazareva, A. Release of engineered nanomaterials from personal care products throughout their life cycle. *J. Nanopart. Res.* **2014**, *16*. [CrossRef]
2. Guo, K.; Han, F.X.; Kingery, W.; Sun, H.; Zhang, J. Development of novel nanomaterials for remediation of heavy metals and radionuclides in contaminated water. *Nanotechnol. Environ. Eng.* **2016**, *1*, 7. [CrossRef]
3. Sun, T.Y.; Bornhöft, N.A.; Hungerbühler, K.; Nowack, B. Dynamic probabilistic modeling of environmental emissions of engineered nanomaterials. *Environ. Sci. Technol.* **2016**, *50*, 4701–4711. [CrossRef] [PubMed]
4. Wang, Z.L. Zinc oxide nanostructures: Growth, properties and applications. *J. Phys. Condens. Matter* **2004**, *16*. [CrossRef]
5. Piccinno, F.; Gottschalk, F.; Seeger, S.; Nowack, B. Industrial production quantities and uses of ten engineered nanomaterials in Europe and the world. *J. Nanopart. Res.* **2012**, *14*, 1109. [CrossRef]
6. Gottschalk, F.; Nowack, B. The release of engineered nanomaterials to the environment. *J. Environ. Monit.* **2011**, *13*, 1145. [CrossRef] [PubMed]
7. Fairbairn, E.A.; Keller, A.A.; Mädler, L.; Zhou, D.; Pokhrel, S.; Cherr, G.N. Metal oxide nanomaterials in seawater: Linking physicochemical characteristics with biological response in sea urchin development. *J. Hazard. Mater.* **2011**, *192*, 1565–1571. [CrossRef] [PubMed]
8. Cupi, D.; Hartmann, N.B.; Baun, A. Influence of pH and media composition on suspension stability of silver, zinc oxide, and titanium dioxide nanoparticles and immobilization of Daphnia magna under guideline testing conditions. *Ecotoxicol. Environ. Saf.* **2016**, *127*, 144–152. [CrossRef] [PubMed]
9. Dreher, K.L. Health and environmental impact of nanotechnology: Toxicological assessment of manufactured nanoparticles. *Toxicol. Sci.* **2004**, *77*, 3–5. [CrossRef] [PubMed]
10. Lin, W.; Xu, Y.; Huang, C.C.; Ma, Y.; Shannon, K.B.; Chen, D.R.; Huang, Y.W. Toxicity of nano- and micro-sized ZnO particles in human lung epithelial cells. *J. Nanopart. Res.* **2009**, *11*, 25–39. [CrossRef]
11. Zhou, D.; Keller, A.A. Role of morphology in the aggregation kinetics of ZnO nanoparticles. *Water Res.* **2010**, *44*, 2948–2956. [CrossRef] [PubMed]
12. Peng, Y.-H.; Tso, C.; Tsai, Y.; Zhuang, C.; Shih, Y. The effect of electrolytes on the aggregation kinetics of three different ZnO nanoparticles in water. *Sci. Total Environ.* **2015**, *530*, 183–190. [CrossRef] [PubMed]
13. Peng, C.; Shen, C.; Zheng, S.; Yang, W.; Hu, H.; Liu, J.; Shi, J. Transformation of CuO Nanoparticles in the Aquatic Environment: Influence of pH, Electrolytes and Natural Organic Matter. *Nanomaterials* **2017**, *7*, 326. [CrossRef] [PubMed]
14. Afshinnia, K.; Gibson, I.; Merrifield, R.; Baalousha, M. The concentration-dependent aggregation of Ag NPs induced by cystine. *Sci. Total Environ.* **2016**, *557–558*, 395–403. [CrossRef] [PubMed]
15. Jiang, C.; Aiken, G.R.; Hsu-Kim, H. Effects of natural organic matter properties on the dissolution kinetics of zinc oxide nanoparticles. *Environ. Sci. Technol.* **2015**, *49*, 11476–11484. [CrossRef] [PubMed]

16. Rupasinghe, R.A. Dissolution and Aggregation of Zinc Oxide Nanoparticles at Circumneutral pH; A Study of Size Effects in the Presence and Absence of Citric Acid. Master's Thesis, University of Iowa, Iowa City, IW, USA, 2011.
17. Khan, R.; Inam, M.; Zam, S.; Park, D.; Yeom, I. Assessment of Key Environmental Factors Influencing the Sedimentation and Aggregation Behavior of Zinc Oxide Nanoparticles in Aquatic Environment. *Water* **2018**, *10*, 660. [CrossRef]
18. Gondikas, A.P.; Morris, A.; Reinsch, B.C.; Marinakos, S.M.; Lowry, G.V.; Hsu-Kim, H. Cysteine-induced modifications of zero-valent silver nanomaterials: Implications for particle surface chemistry, aggregation, dissolution, and silver speciation. *Environ. Sci. Technol.* **2012**, *46*, 7037–7045. [CrossRef] [PubMed]
19. Sun, Q.; Li, Y.; Tang, T.; Yuan, Z.; Yu, C.-P. Removal of silver nanoparticles by coagulation processes. *J. Hazard. Mater.* **2013**, *261*, 414–420. [CrossRef] [PubMed]
20. Wang, H.T.; Ye, Y.Y.; Qi, J.; Li, F.T.; Tang, Y.L. Removal of titanium dioxide nanoparticles by coagulation: Effects of coagulants, typical ions, alkalinity and natural organic matters. *Water Sci. Technol.* **2013**, *68*, 1137–1143. [CrossRef] [PubMed]
21. Hyung, H.; Kim, J.H. Dispersion of C60in natural water and removal by conventional drinking water treatment processes. *Water Res.* **2009**, *43*, 2463–2470. [CrossRef] [PubMed]
22. Zhang, Y.; Chen, Y.; Westerhoff, P.; Crittenden, J.C. Stability and removal of water soluble CdTe quantum dots in water. *Environ. Sci. Technol.* **2007**, *42*, 321–325. [CrossRef]
23. Abbott Chalew, T.E.; Ajmani, G.S.; Huang, H.; Schwab, K.J. Evaluating nanoparticle breakthrough during drinking water treatment. *Environ. Health Perspect.* **2013**, *121*, 1161–1166. [CrossRef] [PubMed]
24. Wang, Y.; Xue, N.; Chu, Y.; Sun, Y.; Yan, H.; Han, Q. CuO nanoparticle–humic acid (CuONP–HA) composite contaminant removal by coagulation/ultrafiltration process: The application of sodium alginate as coagulant aid. *Desalination* **2015**, *367*, 265–271. [CrossRef]
25. Sun, J.; Gao, B.; Zhao, S.; Li, R.; Yue, Q.; Wang, Y.; Liu, S. Simultaneous removal of nano-ZnO and Zn^{2+} based on transportation character of nano-ZnO by coagulation: Enteromorpha polysaccharide compound polyaluminum chloride. *Environ. Sci. Pollut. Res.* **2017**, *24*, 5179–5188. [CrossRef] [PubMed]
26. Mizutani, K.; Fisher-Power, L.M.; Shi, Z.; Cheng, T. Cu and Zn adsorption to a terrestrial sediment: Influence of solid-to-solution ratio. *Chemosphere* **2017**, *175*, 341–349. [CrossRef] [PubMed]
27. Erto, A.; Di Natale, F.; Musmarra, D.; Lancia, A. Modeling of single and competitive adsorption of cadmium and zinc onto activated carbon. *Adsorption* **2015**, *21*, 611–621. [CrossRef]
28. Cheng, T.; Barnett, M.O.; Roden, E.E.; Zhuang, J. Effects of solid-to-solution ratio on uranium(VI) adsorption and its implications. *Environ. Sci. Technol.* **2006**, *40*, 3243–3247. [CrossRef] [PubMed]
29. Sousa, V.S.; Corniciuc, C.; Teixeira, M.R. The effect of TiO_2 nanoparticles removal on drinking water quality produced by conventional treatment C/F/S. *Water Res.* **2017**, *109*, 1–12. [CrossRef] [PubMed]
30. Hong, S.; Elimelech, M. Chemical and physical aspects of natural organic matter (NOM) fouling of nanofiltration membranes. *J. Membr. Sci.* **1997**, *132*, 159–181. [CrossRef]
31. EPA, United States Environmental Protection Agency. *Enhanced Coagulation and Enhanced Precipitative Softening Guidance Manual*; Disinfection Byproducts Byproducts Rule; EPA: Washington, DC, USA, 1999.
32. Edzwald, J.K.; Tobiason, J.E. Enhanced coagulation: US requirements and a broader view. *Water Sci. Technol.* **1999**, *40*, 63–70. [CrossRef]
33. Kato, H.; Fujita, K.; Horie, M.; Suzuki, M.; Nakamura, A.; Endoh, S.; Yoshida, Y.; Iwahashi, H.; Takahashi, K.; Kinugasa, S. Dispersion characteristics of various metal oxide secondary nanoparticles in culture medium for in vitro toxicology assessment. *Toxicol. In Vitro* **2010**, *24*, 1009–1018. [CrossRef] [PubMed]
34. Keller, A.A.; Wang, H.; Zhou, D.; Lenihan, H.S.; Cherr, G.; Cardinale, B.J.; Miller, R.; Zhaoxia, J.I. Stability and aggregation of metal oxide nanoparticles in natural aqueous matrices. *Environ. Sci. Technol.* **2010**, *44*, 1962–1967. [CrossRef] [PubMed]
35. Chen, J.-F.; Zhang, J.-Y.; Shen, Z.-G.; Zhong, J.; Yun, J. Preparation and characterization of amorphous cefuroxime axetil drug nanoparticles with novel technology: High-gravity antisolvent precipitation. *Ind. Eng. Chem. Res.* **2006**, *45*, 8723–8727. [CrossRef]
36. Erhayem, M.; Sohn, M. Stability studies for titanium dioxide nanoparticles upon adsorption of Suwannee River humic and fulvic acids and natural organic matter. *Sci. Total Environ.* **2014**, *468–469*, 249–257. [CrossRef] [PubMed]

37. Wang, H.; Zhao, X.; Han, X.; Tang, Z.; Song, F.; Zhang, S.; Zhu, Y.; Guo, W.; He, Z.; Guo, Q. Colloidal stability of Fe_3O_4 magnetic nanoparticles differentially impacted by dissolved organic matter and cations in synthetic and naturally-occurred environmental waters. *Environ. Pollut.* **2018**, *241*, 912–921. [CrossRef] [PubMed]
38. Koneswaran, M.; Narayanaswamy, R. L-Cysteine-capped ZnS quantum dots based fluorescence sensor for Cu^{2+} ion. *Sens. Actuators B Chem.* **2009**, *139*, 104–109. [CrossRef]
39. Tombácz, E.; Filipcsei, G.; Szekeres, M.; Gingl, Z. Particle aggregation in complex aquatic systems. *Colloids Surf. A Physicochem. Eng. Asp.* **1999**, *151*, 233–244. [CrossRef]
40. Kinsinger, N.; Honda, R.; Keene, V.; Walker, S.L. Titanium Dioxide Nanoparticle Removal in Primary Prefiltration Stages of Water Treatment: Role of Coating, Natural Organic Matter, Source Water, and Solution Chemistry. *Environ. Eng. Sci.* **2015**, *32*, 292–300. [CrossRef]
41. Ravindran, A.; Dhas, S.P.; Chandrasekaran, N.; Mukherjee, A. Differential interaction of silver nanoparticles with cysteine. *J. Exp. Nanosci.* **2013**, *8*, 589–595. [CrossRef]
42. Baalousha, M. Aggregation and disaggregation of iron oxide nanoparticles: Influence of particle concentration, pH and natural organic matter. *Sci. Total Environ.* **2009**, *407*, 2093–2101. [CrossRef] [PubMed]
43. Chibowski, E.; Holysz, L.; Terpilowski, K.; Wiacek, A.E. Influence of ionic surfactants and lecithin on stability of titanium dioxide in aqueous electrolyte solution. *Croat. Chem. Acta* **2007**, *80*, 395–403.
44. Maximova, N.; Dahl, O. Environmental implications of aggregation phenomena: Current understanding. *Curr. Opin. Colloid Interface Sci.* **2006**, *11*, 246–266. [CrossRef]
45. Taboada-Serrano, P.; Chin, C.-J.; Yiacoumi, S.; Tsouris, C. Modeling aggregation of colloidal particles. *Curr. Opin. Colloid Interface Sci.* **2005**, *10*, 123–132. [CrossRef]
46. Zhang, L.; Mao, J.; Zhao, Q.; He, S.; Ma, J. Effect of $AlCl^3$ concentration on nanoparticle removal by coagulation. *J. Environ. Sci.* **2015**, *38*, 103–109. [CrossRef] [PubMed]
47. Liu, N.; Liu, C.; Zhang, J.; Lin, D. Removal of dispersant-stabilized carbon nanotubes by regular coagulants. *J. Environ. Sci.* **2012**, *24*, 1364–1370. [CrossRef]
48. Duan, J.; Gregory, J. Coagulation by hydrolysing metal salts. *Adv. Colloid Interface Sci.* **2003**, *100*, 475–502. [CrossRef]
49. Sharp, E.L.; Jarvis, P.; Parsons, S.A.; Jefferson, B. Impact of fractional character on the coagulation of NOM. *Colloids Surf. Physicochem. Eng. Asp.* **2006**, *286*, 104–111. [CrossRef]
50. Sharp, E.L.; Parson, S.A.; Jefferson, B. Coagulation of NOM: Linking character to treatment. *Water Sci. Technol.* **2006**, *53*, 67–76. [CrossRef] [PubMed]
51. Matilainen, A.; Vepsäläinen, M.; Sillanpää, M. Natural organic matter removal by coagulation during drinking water treatment: A review. *Adv. Colloid Interface Sci.* **2010**, *159*, 189–197. [CrossRef] [PubMed]
52. Joseph, L.; Flora, J.R. V.; Park, Y.-G.; Badawy, M.; Saleh, H.; Yoon, Y. Removal of natural organic matter from potential drinking water sources by combined coagulation and adsorption using carbon nanomaterials. *Sep. Purif. Technol.* **2012**, *95*, 64–72. [CrossRef]
53. Jiang, J.-Q. The role of coagulation in water treatment. *Curr. Opin. Chem. Eng.* **2015**, *8*, 36–44. [CrossRef]
54. Wang, L.; Han, C.; Nadagouda, M.N.; Dionysiou, D.D. An innovative zinc oxide-coated zeolite adsorbent for removal of humic acid. *J. Hazard. Mater.* **2016**, *313*, 283–290. [CrossRef] [PubMed]
55. Matrajt, G.; Borg, J.; Raynal, P.I.; Djouadi, Z.; D'Hendecourt, L.; Flynn, G.J.; Deboffle, D. FTIR and Raman analyses of the Tagish Lake meteorite: Relationship with the aliphatic hydrocarbons observed in the Diffuse Interstellar Medium. *Astron. Astrophys.* **2004**, *416*, 983–990. [CrossRef]
56. Vlachos, N.; Skopelitis, Y.; Psaroudaki, M.; Konstantinidou, V.; Chatzilazarou, A.; Tegou, E. Applications of Fourier transform-infrared spectroscopy to edible oils. *Anal. Chim. Acta* **2006**, *573–574*, 459–465. [CrossRef] [PubMed]
57. Sun, W.-L.; Xia, J.; Li, S.; Sun, F. Effect of natural organic matter (NOM) on Cu (II) adsorption by multi-walled carbon nanotubes: Relationship with NOM properties. *Chem. Eng. J.* **2012**, *200*, 627–636. [CrossRef]
58. Inam, M.A.; Khan, R.; Park, D.R.; Lee, Y.-W.; Yeom, I.T. Removal of Sb (III) and Sb (V) by Ferric Chloride Coagulation: Implications of Fe Solubility. *Water* **2018**, *10*, 418. [CrossRef]
59. Liao, Y.; Tang, X.; Yang, Q.; Chen, W.; Liu, B.; Zhao, C.; Zhai, J.; Zheng, H. Characterization of an inorganic polymer coagulant and coagulation behavior for humic acid/algae-polluted water treatment: Polymeric zinc–ferric–silicate–sulfate coagulant. *RSC Adv.* **2017**, *7*, 19856–19862. [CrossRef]
60. Sandmann, A.; Kompch, A.; Mackert, V.; Liebscher, C.H.; Winterer, M. Interaction of l-cysteine with ZnO: Structure, surface chemistry, and optical properties. *Langmuir* **2015**, *31*, 5701–5711. [CrossRef] [PubMed]

61. Li, R.; He, C.; He, Y. Preparation and characterization of poly-silicic-cation coagulants by synchronous-polymerization and co-polymerization. *Chem. Eng. J.* **2013**, *223*, 869–874. [CrossRef]
62. Moussas, P.A.; Zouboulis, A.I. A study on the properties and coagulation behaviour of modified inorganic polymeric coagulant—Polyferric silicate sulphate (PFSiS). *Sep. Purif. Technol.* **2008**, *63*, 475–483. [CrossRef]
63. Tsyganenko, A.A.; Lamotte, J.; Saussey, J.; Lavalley, J.C. Bending vibrations of OH groups resulting from H_2 dissociation on ZnO. *J. Chem. Soc. Faraday Trans. 1 Phys. Chem. Condens. Phases* **1989**, *85*, 2397–2403. [CrossRef]
64. Pinotti, A.; Zaritzky, N. Effect of aluminum sulfate and cationic polyelectrolytes on the destabilization of emulsified wastes. *Waste Manag.* **2001**, *21*, 535–542. [CrossRef]

© 2018 by the authors. Licensee MDPI, Basel, Switzerland. This article is an open access article distributed under the terms and conditions of the Creative Commons Attribution (CC BY) license (http://creativecommons.org/licenses/by/4.0/).